10 min, transferred to a fresh tube and then neutralized with Tris–HCl (pH 9.1). The eluted phage were titred and binding efficiency was compared.

The phage eluted after third-round substrate exposure were mixed with their *Escherichia coli* ER2537 host and plated on LB XGal/IPTG plates. Since the library phage were derived from the vector M13mp19, which carries the lacZα gene, phage plaques were blue in colour when plated on media containing Xgal (5-bromo-4-chloro-3-indoyl-β-D-galactoside) and IPTG (isopropyl-β-D-thiogalactoside). Blue/white screening was used to select phage plaques with the random peptide insert. Plaques were picked and DNA sequenced from these plates.

Substrate preparation

Substrate orientations were confirmed by X-ray diffraction, and native oxides were removed by appropriate chemical specific etching. The following etches were tested on GaAs and InP surfaces: NH_4OH: H_2O 1:10, HCl:H_2O 1:10, H_3PO_4: H_2O_2: H_2O 3:1:50 at 1 min and 10 min etch times. The best element ratio and least oxide formation (using XPS) for GaAs and InP etched surfaces was achieved using HCl: H_2O for 1 min followed by a deionized water rinse for 1 min. However, since an ammonium hydroxide etch was used for GaAs in the initial screening of the library, this etch was used for all other GaAs substrate experiments. Si(100) wafers were etched in a solution of HF:H_2O 1:40 for one minute, followed by a deionized water rinse. All surfaces were taken directly from the rinse solution and immediately introduced to the phage library. Surfaces of control substrates, not exposed to phage, were characterized and mapped for effectiveness of the etching process and morphology of surfaces by AFM and XPS.

Multilayer substrates of GaAs and of $Al_{0.98}Ga_{0.02}As$ were grown by molecular beam epitaxy onto (100) GaAs. The epitaxially grown layers were Si-doped (n-type) at a level of 5×10^{17} cm^{-3}.

Antibody and gold labelling

For the XPS, SEM and AFM experiments, substrates were exposed to phage for 1 h in Tris-buffered saline then introduced to an anti-fd bacteriophage—biotin conjugate, an antibody to the pIII protein of fd phage, (1:500 in phosphate buffer, Sigma) for 30 min and then rinsed in phosphate buffer. A streptavidin/20-nm colloidal gold label (1:200 in phosphate buffered saline (PBS), Sigma) was attached to the biotin conjugated phage through a biotin–streptavidin interaction; the surfaces were exposed to the label for 30 min and then rinsed several times with PBS.

XPS

The following controls were done for the XPS experiments to ensure that the gold signal seen in XPS was from gold bound to the phage and not non-specific antibody interaction with the GaAs surface. The prepared (100) GaAs surface was exposed to (1) antibody and the streptavidin–gold label, but without phage, (2) G1-3 phage and streptavidin–gold label, but without the antibody, and (3) streptavidin–gold label, without either G1-3 phage or antibody.

The XPS instrument used was a Physical Electronics Phi ESCA 5700 with an aluminium anode producing monochromatic 1,487-eV X-rays. All samples were introduced to the chamber immediately after gold-tagging the phage (as described above) to limit oxidation of the GaAs surfaces, and then pumped overnight at high vacuum to reduce sample outgassing in the XPS chamber.

AFM

The AFM used was a Digital Instruments Bioscope mounted on a Zeiss Axiovert 100s-2tv, operating in tip scanning mode with a G scanner. The images were taken in air using tapping mode. The AFM probes were etched silicon with 125-μm cantilevers and spring constants of 20–100 $N\,m^{-1}$ driven near their resonant frequency of 200–400 kHz. Scan rates were of the order of 1–5 $\mu m\,s^{-1}$. Images were levelled using a first-order plane fit to remove sample tilt.

TEM

TEM images were taken using a Philips EM208 at 60 kV. The G1-3 phage (diluted 1:100 in TBS) were incubated with GaAs pieces (500 μm) for 30 min, centrifuged to separate particles from unbound phage, rinsed with TBS, and resuspended in TBS. Samples were stained with 2% uranyl acetate.

SEM

The G12-3 phage (diluted 1:100 in TBS) were incubated with a freshly cleaved heterostructure surface for 30 min and rinsed with TBS. The G12-3 phage were tagged with 20-nm colloidal gold. SEM and elemental mapping images were collected using the Norian detection system mounted on a Hitachi 4700 field emission scanning electron microscope at 5 kV.

Received 16 November 1999; accepted 10 April 2000.

1. Belcher, A. M. *et al.* Control of crystal phase switching and orientation by soluble mollusc-shell proteins. *Nature* **381,** 56–58 (1996).
2. Falini, G. *et al.* Control of aragonite or calcite polymorphism by mollusk shell macromolecules. *Science* **271,** 67–69 (1996).
3. Cha, J. N. Silicatein filaments and subunits from a marine sponge direct the polymerization of silica and silicones *in vitro*. *Proc. Natl Acad. Sci. USA* **96,** 361–365 (1999).
4. Meldrum, F. C., Mann, S., Heywood, B. R., Frankel, R. B. & Bazylinski, D. A. Electron microscopy study of magnetosomes in two cultured vibrioid magnetotactic bacteria. *Proc. R. Soc. Lond. B* **251,** 238–242 (1993).
5. Colvin, V. L., Goldstein, A. N. & Alivisatos, A. P. Semiconductor nanocrystals covalently bound to metal surfaces with self-assembled monolayers. *J. Am. Chem. Soc.* **144,** 5221–5230 (1992).
6. Brust, M., Bethell, D., Schiffrin, D. J. & Kiely, C. J. Novel gold-dithiol nano-networks with nonmetal electronic properties. *Adv. Mater.* **7,** 795–797 (1995).
7. Li, M., Wong, K. K. W. & Mann, S. Organization of inorganic nanoparticles using biotin-streptavidin connectors. *Chem. Mater.* **11,** 23–26 (1999).
8. Alivisatos, A. P. *et al.* Organization of 'nanocrystal molecules' using DNA. *Nature* **382,** 609–611 (1996).
9. Mirkin, C. A., Letsinger, R. L., Mucic, R. C. & Storhoff, J. J. A DNA-based method for rationally assembling nanoparticles into macroscopic materials. *Nature* **382,** 607–609 (1996).
10. Brown, S. Engineered iron oxide-adhesion mutants of the *Escherichi coli* phage λ receptor. *Proc. Natl Acad. Sci. USA* **89,** 8651–8655 (1992).
11. Brown, S. Metal-recognition by repeating polypeptides. *Nature Biotechnol.* **15,** 269–272 (1997).
12. Parmley, S. F. & Smith, G. P. Antibody-selectable filamentous Fd phage vectors- affinity purification of target genes. *Gene* **73,** 305–318 (1988).
13. Swaminathan, V. & Macrander, A. T. *Materials Aspects of GaAs and InP Based Structures* (Prentice Hall, Englewood Cliffs, New Jersey, 1991).

Acknowledgements

We thank D. Margolese, D. Morse and G. Stucky for discussions, and H. Reese, J. English and R. Naone for providing semiconductor substrates. We acknowledge the use of the core microscopy facilities in the Texas Materials Institute (SEM). We also thank the Institute of Molecular and Cellular Biology (TEM) at the University of Texas at Austin. We acknowledge the assistance of the NSF-sponsored National Nanofabrication Users Network in providing some of the structures for this project. This work was supported by ARO/DARPA (S.R.W and A.M.B), a DuPont Young Investigator Award (A.M.B.), the NSF (P.F.B. and E.L.H.) and the Robert A. Welch Foundation (P.F.B. and A.M.B.). This work was also funded by faculty start-up funds provided by the University of Texas at Austin (A.M.B.).

Correspondence and requests for materials should be addressed to A.M.B. (e-mail: belcher@mail.utexas.edu).

Reduced growth of Alaskan white spruce in the twentieth century from temperature-induced drought stress

Valerie A. Barber*†‡, Glenn Patrick Juday†‡ & Bruce P. Finney*

** Institute of Marine Science, † Forest Sciences Department, University of Alaska Fairbanks, Fairbanks, AK 99775, USA*
‡ These authors contributed equally to the work

The extension of growing season at high northern latitudes seems increasingly clear from satellite observations of vegetation extent and duration[1,2]. This extension is also thought to explain the observed increase in amplitude of seasonal variations in atmospheric CO_2 concentration. Increased plant respiration and photosynthesis both correlate well with increases in temperature this century and are therefore the most probable link between the vegetation and CO_2 observations[3]. From these observations[1,2], it has been suggested that increases in temperature have stimulated carbon uptake in high latitudes[1,2] and for the boreal forest system as a whole[4]. Here we present multi-proxy tree-ring data (ring width, maximum late-wood density and carbon-isotope composition) from 20 productive stands of white spruce in the interior of Alaska. The tree-ring records show a strong and consistent relationship over the past 90 years and indicate that, in contrast with earlier predictions, radial growth has decreased with increasing temperature. Our data show that temperature-induced drought stress has disproportionately affected the most rapidly growing white spruce, suggesting that, under recent climate warming, drought may have been an important factor limiting carbon uptake in a large portion of the North American boreal forest. If this limitation in growth due to drought stress is sustained, the future capacity of northern latitudes to sequester carbon may be less than currently expected.

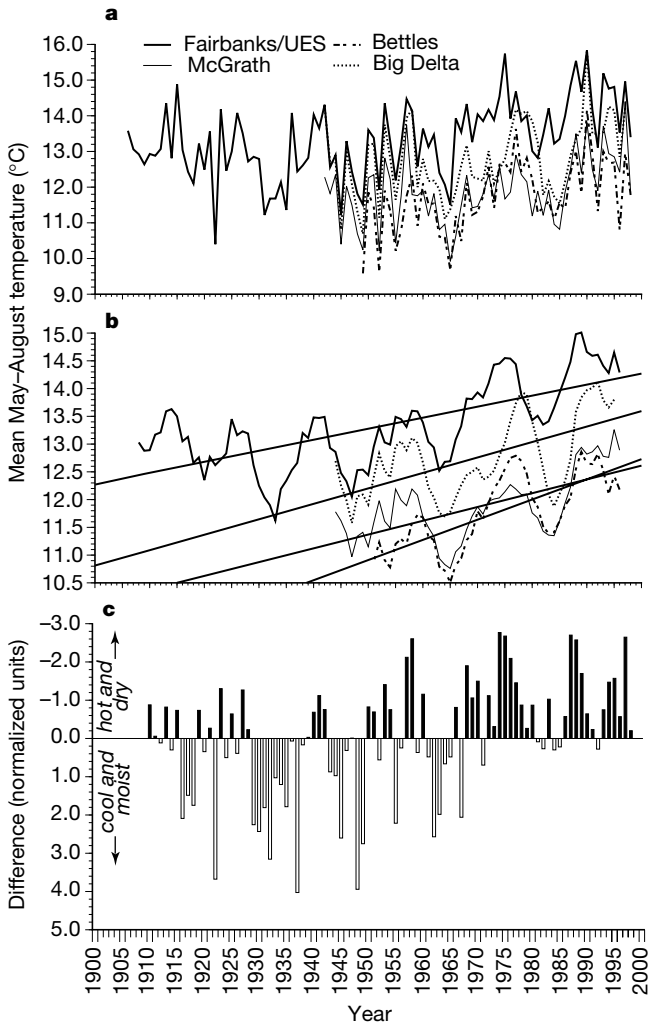

Figure 1 Climate trends in interior Alaska in the twentieth century. Mean summer (May through August) temperature at four meteorological stations (see Fig. 2 for locations). **a**, annual values; **b**, annual values smoothed with five-year running mean and fitted with regression line; **c**, normalized growth year (September through August) precipitation minus normalized May through August temperature at Fairbanks. Scaled to zero mean over the period 1906–98.

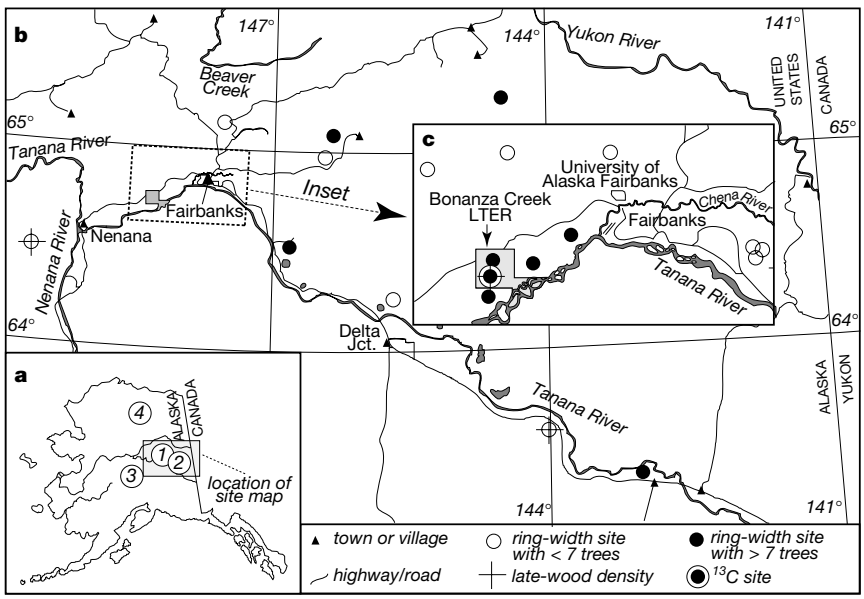

Figure 2 Map of field area. **a**, Location of meteorological stations. Numbered circles represent meteorological stations: 1, Fairbanks/University Experiment Station; 2, Big Delta; 3, McGrath; 4, Bettles. **b**, Extensive tree-ring sampling sites in east-central Alaska. **c**, Inset of intensive tree-ring sampling locations in and near Bonanza Creek Long-term Ecological Research (LTER). See legend for **b** and **c**.

We assembled the available twentieth-century summer climate records from stations representative of the boreal forest region of Alaska (Fig. 1a, b). Although the greatest magnitude of high latitude warming has been reported in winter and early spring[5], these Alaska stations show a strong warming trend in the growing season over the past 50 years (Fig. 1a, b). Interior Alaska is semi-arid with potential evapotranspiration equal to annual precipitation at many interior locations[6]. A combined index of growing season temperature and growth-year precipitation in central Alaska registers severe and prolonged warmth and dryness from the 1970s to the present that is unprecedented in the twentieth century (Fig. 1c). Warming without a concurrent increase in precipitation is projected to turn regions of the present-day central Canadian boreal forest into lower productivity Aspen parklands[7].

We sampled trees from a broad range of diameters from closed-canopy white spruce stands in the Bonanza Creek Long-Term Ecological Research site and surrounding areas across east-central Alaska (Fig. 2). The sample represents mature and old stands (Fig. 3a) representative of the Alaskan boreal forest, in contrast to the well studied forest–tundra treeline[8–10].

Correlation analyses of all three tree-ring parameters for 36 months (year of tree-ring formation plus the two years before) with the Fairbanks/University Experiment Station record show highly significant correlation with summer temperatures (Fig. 4a–c). We did not use other interior Alaska climate stations because they are highly correlated with the Fairbanks record (Fig. 1) and are shorter in duration. Ring-width is strongly negatively correlated with summer monthly mean temperature in the year of ring formation plus the two years before (Fig. 4a). The negative relationship of ring-width and summer temperature contrasts with the positive relationship widely reported for forest-tundra margin trees[8,10,11]. Growth-year precipitation (September through August) is correlated positively ($p > 0.01$) with ring-width both for the year of ring formation (0.34 annual values, 0.64 for five-year running mean (smoothed)) and the year before (0.39 annual values, 0.68 smoothed). Most conifers are determinate growers: photosynthetic gain in the growth season before ring formation has the strongest influence on current-year growth[12]. By contrast, the $\delta^{13}C$ and maximum late-wood density (MLWD) properties in spruce ring-width are correlated most strongly with mean monthly summer temperatures of the current growth year (Fig. 4b, c).

We combined monthly mean summer temperature and growth year precipitation into an index of climatic favourability for white spruce growth (see Methods). High radial growth and favourable climate occur consistently during the 50-year period 1915–65 (Fig. 5a). The ring-width climate index (CI_{rw}) closely mirrors one- and two-year positive and negative growth anomalies in the sample (Fig. 5a), such as the spike of growth in response to a cool and moist 1937 and the short, sharp reduction of growth in

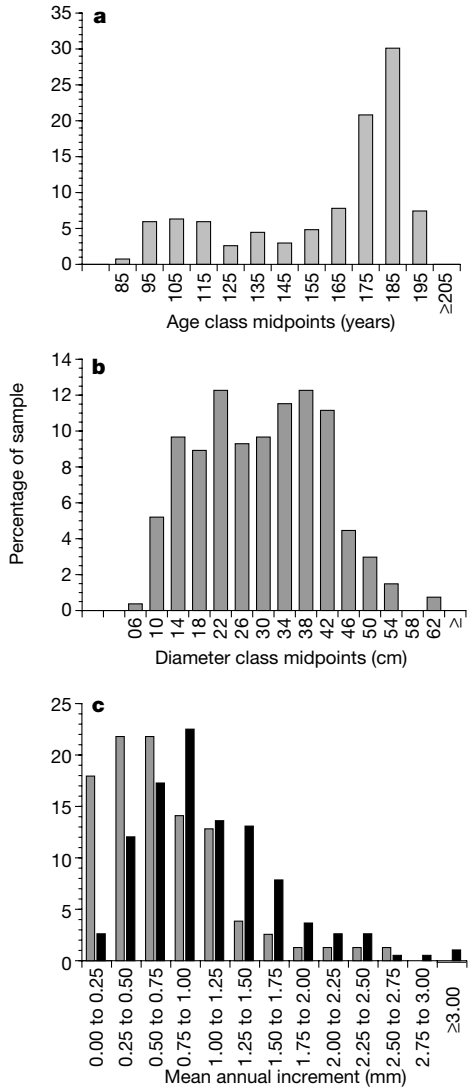

Figure 3 Characteristics of white spruce radial-growth sample. **a**, **b**, Minimum tree age (**a**) and diameter (**b**), $n = 269$ trees. **c**, Frequency distribution of twentieth-century radial growth for trees correlated ($p < 0.05$) with Fairbanks ring-width climate index ($n = 191$) (black bars) and trees not correlated ($p > 0.05$) with ring-width climate index ($n = 78$) (grey bars).

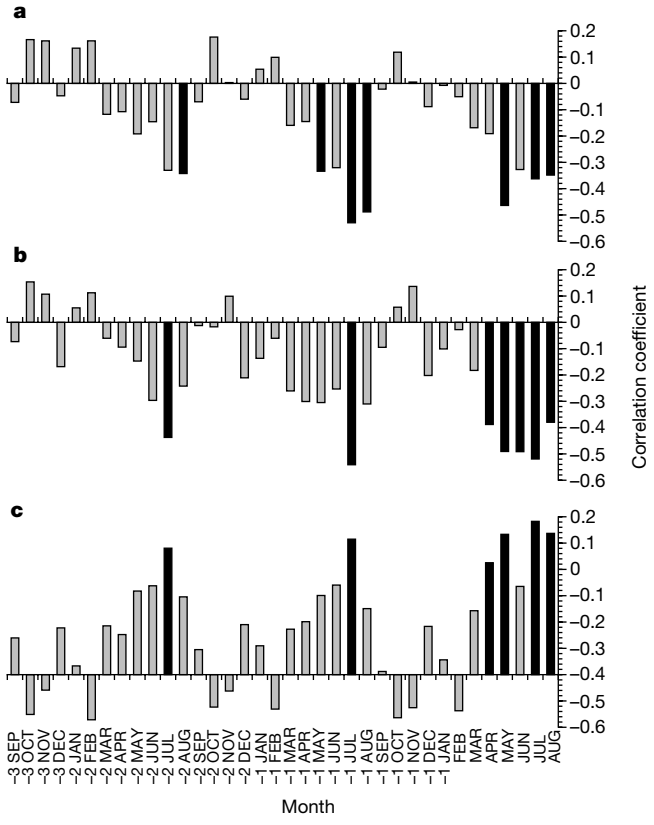

Figure 4 Correlation of tree-ring properties to Fairbanks mean monthly temperature for the three years before completion of tree-ring growth. The year is indicated by a number from –1 to –3. All values are Pearson correlation coefficients; correlations significant at $p < 0.01$ are shaded black. **a**, Ring width; **b**, $\delta^{13}C$ discrimination; **c**, maximum late-wood density. Correlation values are for the period 1909–1996 (**a** and **b**) and 1918–94 (**c**).

response to the warm and dry years of 1957–58 (Fig. 1c). A quasi-decadal cyclicity is apparent in which opposite trends in mean radial growth occur regularly over periods of 5–6 years (Fig. 5a, b). The most striking feature of the climate and ring-width record is the sustained unfavourable climate signal and growth response from the 1970s to the present.

Several features of the sample indicate that this climatically related growth reduction is significant at the landscape level of carbon uptake. Mean ring-width of each of the 20 stands and radial growth of a majority (71%) of the individual trees in the sample are significantly correlated ($p > 0.05$) with CI_{rw}. The population of trees that is significantly correlated with climate displays a distribution skewed towards faster rates of growth in the twentieth century than the portion of the population that is not significantly correlated (Fig. 3c). Thus the fastest growing trees are most limited by summer warmth and low precipitation.

Correlation analyses of the $\delta^{13}C$ and wood density properties provide independent confirmation of the ring-width results. The carbon-isotope ($\delta^{13}C$) ratio provides information on CO_2 uptake and water vapour loss during photosynthesis[13], and thus under limiting conditions can register drought stress. We calculated discrimination of $\delta^{13}C$, the difference between $\delta^{13}C$ of the tree-ring (hollocellulose) and atmospheric $\delta^{13}C$ annually. The $\delta^{13}C$ discrimination of our sampled white spruce is significantly negatively correlated with summer monthly mean temperatures in the year of the ring formation (Fig. 4b).

Fairbanks precipitation is significantly correlated with $\delta^{13}C$ discrimination (0.335, $p > 0.02$), but combining summer temperature with growth-year precipitation did not result in a significantly higher overall correlation than the correlation with summer temperature alone. The $\delta^{13}C$ discrimination of white spruce displays a strong relationship to the short-term variability of Fairbanks summer temperature throughout the twentieth century (Fig. 5c) and declines in the 1980s and 1990s to an unprecedented and sustained low level for the twentieth century (Fig. 5d).

MLWD is the maximum density of the wood formed at the end of the growing season when conifer tracheids switch from large-diameter, thin-walled cells (formed in spring and early summer) to smaller-diameter, thick-walled cells. Correlation analysis has shown that this number integrates growing conditions over the length of the photosynthetically active season[14] and is also more consistent than ring-width[15]. We hypothesize that an increase in the length of the growing season along with warmer summer temperatures depletes already limiting soil moisture. In an environment of high soil-moisture tension, wood cell production shifts earlier in the summer from relatively low-density early wood to higher-density late wood, prolonging the wall-thickness phase of growth which is associated with increased late-wood density[16,17]. The MLWD of our white spruce sample is significantly correlated with early and late summer temperatures in the year of ring formation (Fig. 4c), as

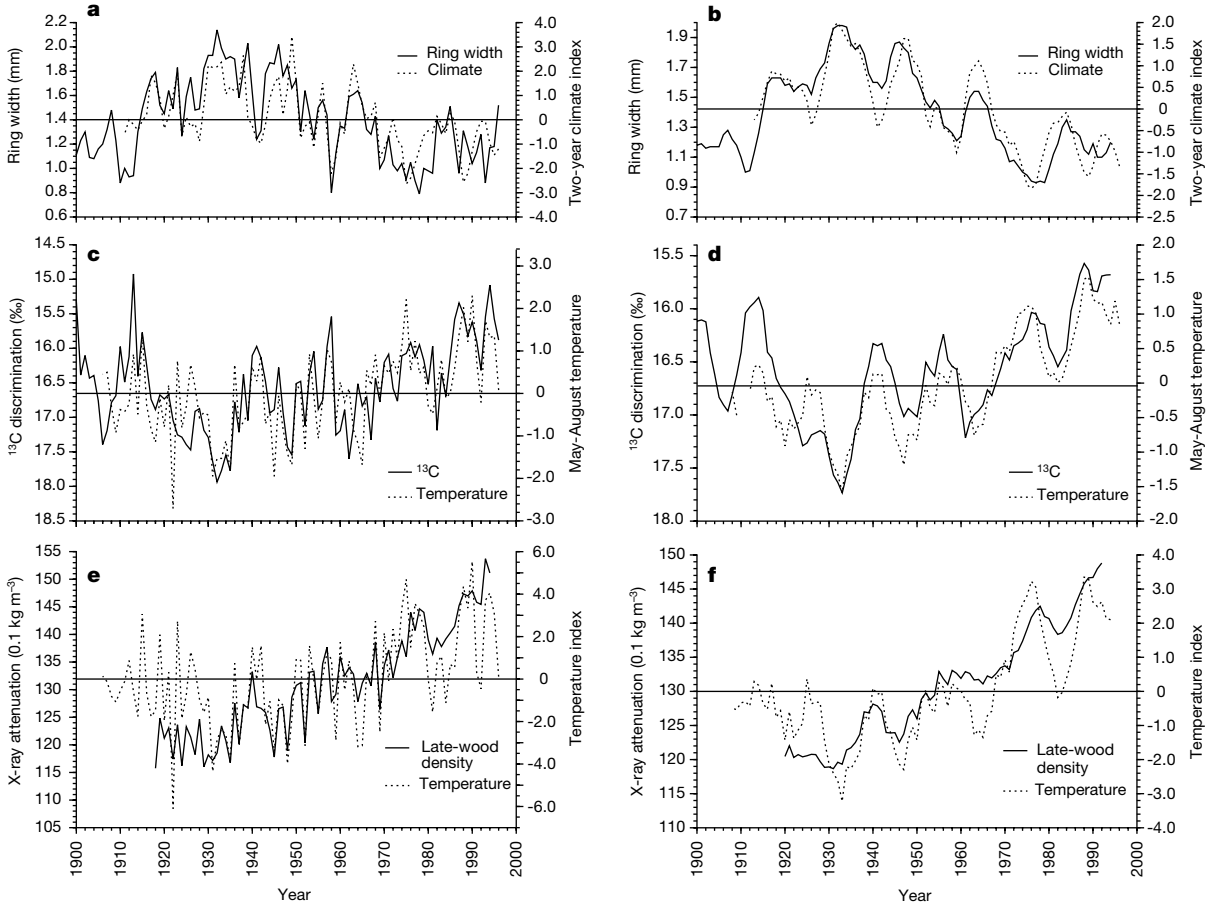

Figure 5 Tree-ring properties in relation to Fairbanks climate during the twentieth century. Annual values on left, smoothed (five-year running mean) on right. All climate values are normalized with zero mean and scaled as standard deviation units. All correlations are significant at $p < 0.001$. **a**, Ring-width versus two-year average Fairbanks climate index (see Methods for definition of ring-width climate index; see Fig. 1c for one-year values of ring-width climate index), correlation = 0.75. **b**, Smoothed ring-width and climate index, correlation = 0.91. **c**, $\delta^{13}C$ discrimination versus May through August temperature, correlation = 0.69. **d**, Smoothed $\delta^{13}C$ discrimination and May through August temperature, correlation = 0.85. **e**, Maximum late-wood density versus density climate index (mean of normalized May, July and August temperature), correlation = 0.75. **f**, smoothed maximum late-wood density and density climate index, correlation = 0.92.

noted for North American treeline white spruce[15], and other months add little improvement. An unprecedented late-twentieth-century rise in MLWD and the associated temperature index is consistent with the other tree-ring properties (Fig. 5e, f).

Our carbon isotope and MLWD results confirm that drought stress accounts for the climate sensitivity of ring-width for productive upland white spruce sites in interior Alaska. Climate sensitivity in our sample has been sustained (neither degraded nor improved) over the last nine decades, and drought stress has reached levels unprecedented in the twentieth century because of climate warming experienced in the 1980s and 1990s. The wide distribution (Fig. 2), representative diameter distribution of the sampled tree population (Fig. 3a, b) and consistent response of the stands suggest that this response is typical of upland white spruce forests in interior Alaska. In the western Canadian boreal forest, white spruce radial growth displays a negative relationship with the duration of fire weather (hot and dry)[18], suggesting that our findings have broader applicability. Our results are also consistent with the suggestion that drought stress is one possible explanation for a late-twentieth-century decrease in the positive relationship of temperature and radial growth of trees at the forest–tundra margin across the Northern Hemisphere[19,20].

White spruce is one of the most productive and widespread forest types in the boreal forest of western North America[21–23]. Thus any coherent, climate-related change in white spruce growth is likely to be an important factor in CO_2 uptake in the boreal forest, a region that is one of the planet's major potential carbon sinks. Our results suggest that the current assumption of carbon-cycle models[24], of a uniform positive relationship of atmospheric carbon uptake to high-latitude warming, will lead to an overestimate of high-latitude carbon storage and an underestimate of future atmospheric CO_2. □

Methods

The radial-growth sample is representative of trees in mature and old stands that are dominant on the contemporary landscape, including trees across a broad range of diameters. The radial-growth sample includes 269 trees in 20 separate stands; radial growth was calculated as a stand-weighted mean. All trees contributed from 1908 until the date of sampling (sampling took place between 1994 and 1996) or, in two cases, the death of the stand. One stand (Reserve West in Bonanza Creek) was killed by wildfire in 1983 and the other was logged in 1987. In these two stands wood disks were harvested from the stumps. Density was measured in cores from 23 trees collected in three stands including Reserve West and outlying sites to the east and west (Fig. 2). The common period of analysis for density was 1918–1994; all trees contributed throughout, except that sample depth in one stand dropped from 14 to 6 trees between 1982 and 1994. Stable carbon isotope ($\delta^{13}C$) was measured only at Reserve West. Four orthogonal cores from each of four trees pooled together give an isotope value representative of a site[25]. We obtained isotope measurements for the period 1900–1981 from four orthogonal wedges from each of four harvested stump disks. For the period 1982–96 samples were obtained from four cores collected at each of four surviving trees near the fire perimeter. We believe the isotope sample is representative of white spruce of the interior Alaskan boreal forest because Reserve West is centrally located, is within the well studied Long-term Ecological Research site, and the tree-ring parameters are well correlated with each other. We confirmed the trends in $\delta^{13}C$ seen at Reserve West in limited samples covering three and four decades collected at two other sites located about 30 km from Bonanza Creek.

We did not transform ring widths into de-trended normalized ring-width index values for two reasons. First, we wanted to preserve the weighting effect of tree increments of different sizes because this reflects annual production more closely than normalized values, which remove this effect. Second, most white spruce of the age range in this study exhibit little age-related growth trend, and the removal of trend is user-specified and risks the loss of information on long-term climate variability that may actually influence tree growth[26]. However, we also correlated climate with de-trended ring-width indices[27] for several stands and found little difference, demonstrating that our results are not an artefact of age-related changes in ring width.

We examined various combinations of climate parameters in order to produce climate indices that maximized correlation for each of the three tree-ring properties (Fig. 5). The climate index (CI_{rw}) that correlates best with ring-width (Fig. 5a, b) is composed of the following parameters:

$$CI_{rw} = (Yr_0(PPT_{gr})_n - (T_{M-A})_n) + Yr_{-1}(PPT_{gr})_n - (T_{M-A})_n))/2$$

where Yr_0 is the year of ring formation, Yr_{-1} is the year prior to ring formation, $(PPT_{gr})_n$ is the normalized growth year precipitation, and $(T_{M-A})_n$ is the normalized May–August temperature.

For stable carbon isotope analysis, four orthogonal samples of annual rings were excised, ground and blended with the same-year wood from four tree disks. Hollocellulose was extracted from the annual wood[28] and carbon-isotope ratios were analysed for the years 1900–81. The same procedure was used on cores from the surviving trees for the period 1967–96, to provide an overlap period for correction. Isotope trends for the period of 1967–81 follow similar curves from both sets of wood samples, but there is a slight offset (0.7) in the $\delta^{13}C$ of the fire-killed trees versus the live trees, probably due to site-specific effects. A correction was made for this offset. A correction was also made for $\delta^{13}C$ changes in atmospheric CO_2 over the last 150 years due to fossil fuel and biomass combustion using the Law Dome Antarctic ice core data (1.53‰ over 150 years) and discrimination was calculated[29]. Thus a continuous record of $\delta^{13}C$ discrimination was determined for 1900–96 and the best correlation was found with May–August temperatures (Fig. 4b, 5c, d).

Maximum late-wood density was measured by X-ray attenuation[15,30] at Lamont-Doherty Earth Observatory. One to four radial samples were collected from each tree. Annual density values were first combined to produce annual tree averages that were then used to calculate overall yearly stand means for each of three stands. The three-stand means were then averaged to produce the sample mean used in correlation analysis. We determined that MLWD correlated best with May, July and August temperatures (Fig. 4c, 5e, f).

Received 25 August 1999; accepted 10 April 2000.

1. Keeling, C. D., Chin, J. F. S. & Whorf, T. P. Increased activity of northern vegetation inferred from atmospheric CO_2 measurements. *Nature* **382,** 146–149 (1996).
2. Myneni, R. B., Keeling, C. D., Tucker, C. J., Asrar, G. & Nemani, R. R. Increased plant growth in the northern high latitudes from 1981–1991. *Nature* **386,** 698–702 (1997).
3. Chapin, F. S. I., ZImov, S. A., Shaver, G. R. & Hobbie, S. E. CO_2 fluctuation at high latitudes. *Nature* **383,** 585–586 (1996).
4. Braswell, B. H., Schimel, D. S., Linder, E. & Moore III, B. The response of global terrestrial ecosystems to interannual temperature variability. *Science* **278,** 870–872 (1997).
5. Chapman, W. L. & Walsh, J. E. Recent variations of sea ice and air temperature in high latitudes. *Bull. Am. Meteorol. Soc.* **74,** 33–47 (1993).
6. Patric, J. H. & Black, P. E. *Potential Evapotranspiration and Climate in Alaska by Thornthwaite's Classification.* (USDA Forest Service Research Paper PNW-71, Juneau, Alaska, 1968).
7. Hogg, E. H. & Hurdle, P. A. The aspen parkland in western Canada: a dry-climate analogue for the future boreal forest? *Wat. Air Soil Pollut.* **82,** 391–400 (1995).
8. Jacoby, G. C. & D'Arrigo, R. Reconstructed northern hemisphere annual temperature since 1671 based on high-latitude tree-ring data from North America. *Clim. Change* **14,** 39–59 (1989).
9. Jacoby, G. C., D'Arrigo, R. D. & Juday, G. P. Tree-ring indicators of climatic change at northern latitudes. *World Res. Rev.* **11,** 21–29 (1999).
10. Garfinkle, H. L. & Brubaker, L. B. Modern climate–tree-growth relationships and climatic reconstruction in sub-Arctic Alaska. *Nature* **286,** 872–874 (1980).
11. Jacoby, G. C., D'Arrigo, R. D. & Davaajamts, T. Mongolian tree rings and 20th-Century warming. *Science* **273,** 771–773 (1996).
12. Kozlowski, T. T. & Pallardy, S. G. *Physiology of Woody Plants* 1–411 (Academic Press, San Diego, California, 1997).
13. Livingston, N. J. & Spittlehouse, D. L. Carbon isotope fractionation in tree rings early and late wood in relation to intra-growing season water balance. *Plant Cell Environ.* **19,** 768–774 (1996).
14. Jacoby, G. C., Ivanciu, I. S. & Ulan, L. D. A 263-year record of summer temperature for northern Quebec reconstructed from tree-ring data and evidence of a major climatic shift in the early 1800's. *Palaeogeogr. Palaeoclimatol. Palaeoecol.* **64,** 69–78 (1988).
15. D'Arrigo, R. D., Jacoby, G. C. & Free, R. M. Tree-ring width and maximum latewood density at the North American tree line: parameters of climate change. *Can. J. Forest Res.* **22,** 1290–1296 (1992).
16. Denne, M. P. Effects of environmental change on wood production and wood structure in *Picea sitchensis* seedlings. *Ann. Bot.* **40,** 1017–1028 (1976).
17. Conkey, L. E. Red spruce tree-ring widths and densities in eastern North America as indicators of past climate. *Quat. Res.* **26,** 232–243 (1986).
18. Larsen, C. P. S. & MacDonald, G. M. Relations between tree-ring widths, climate, and annual area burned in the boreal forest of Alberta. *Can. J. Forest Res.* **25,** 1746–1755 (1995).
19. Jacoby, G. C. & D'Arrigo, R. D. Tree ring width and density evidence of climatic and potential forest change in Alaska. *Glob. Biogeochem. Cycles* **9,** 227–234 (1995).
20. Briffa, K. R. *et al.* Reduced sensitivity of recent tree-growth to temperature at high northern latitudes. *Nature* **391,** 678–682 (1998).
21. Elliott-Fisk, D. L. in *North American Terrestrial Vegetation* (eds Barbour, M. C. & Billings, W. D.) 33–62 (Cambridge University Press, Cambridge, 1988).
22. Ruess, R. W., Van Cleve, K., Yarie, J. & Viereck, L. A. Comparative estimates of fine root production in successional taiga forests on the Alaskan interior. *Can. J. Forest Res.* **26,** 1326–1336 (1996).
23. Van Cleve, K., Chapin III, F. S., Flanagan, P. W., Viereck, L. A. & Dyrness, C. T. *Forest Ecosystems in the Alaskan Taiga: A Synthesis of Structure and Function* 230 (Springer, New York, 1986).
24. Kicklighter, D. W. *et al.* A first-order analysis of the potential role of CO_2 fertilization. *Tellus B* **51,** 343–366 (1999).
25. Leavitt, S. W. & Long, A. Sampling strategy for stable carbon isotope analysis of tree-rings in pine. *Nature* **311,** 145–147 (1984).
26. Briffa, K. R. & Osborn, T. J. Seeing the wood from the trees. *Science* **284,** 926–927 (1999).
27. Cook, E. R. & Kairiukstis, L. A. *Methods of Dendrochronology: Applications in the Environmental Sciences* (Kluwer Academic, Dordrecht, The Netherlands, 1990).
28. Leavitt, S. W. & Danzer, S. R. Method for batch processing small wood samples to holocellulose for stable-carbon isotope analysis. *Anal. Chem.* **65,** 87–89 (1992).
29. Francey, R. J. *et al.* A 1000-year high precision record of $\delta^{13}C$ in atmospheric CO_2. *Tellus B* **51,** 170–193 (1999).
30. Thetford, R. D., D'Arrigo, R. D. & Jacoby, G. C. An image analysis system for determining densitometric and ring-width time series. *Can. J. Forest Res.* **21,** 1544–1548 (1991).

Acknowledgements

This work was carried out with the financial support of the McIntire–Stennis Cooperative

Forestry Research Program, the US NSF Long-Term Ecological Research (LTER) Program and Paleoclimates from Arctic Lakes and Estuaries (PALE) Program, the University of Alaska's Natural Resource Fund, International Arctic Research Centre (IARC), and the Centre for Global Change and Arctic System Research. We thank T. Chapin for enthusiastic support and helpful review of this manuscript. We also thank G. Jacoby for use of his laboratory and equipment for density analyses, and A. Krumhardt for field and laboratory assistance.

Correspondence and requests for materials should be addressed to V.A.B. (e-mail: barber@ims.uaf.edu).

Isotopic evidence for Late Cretaceous plume–ridge interaction at the Hawaiian hotspot

Randall A. Keller*, Martin R. Fisk* & William M. White†

* *College of Oceanic and Atmospheric Sciences, Oregon State University, Corvallis, Oregon 97331, USA*
† *Department of Geological Sciences, Cornell University, Ithaca, New York 14853, USA*

When a mantle plume interacts with a mid-ocean ridge, both are noticeably affected. The mid-ocean ridge can display anomalously shallow bathymetry, excess volcanism, thickened crust, asymmetric sea-floor spreading and a plume component in the composition of the ridge basalts[1–4]. The hotspot-related volcanism can be drawn closer to the ridge, and its geochemical composition can also be affected[3,5–7]. Here we present Sr–Nd–Pb isotopic analyses of samples from the next-to-oldest seamount in the Hawaiian hotspot track, the Detroit seamount at 51° N, which show that, 81 Myr ago, the Hawaiian hotspot produced volcanism with an isotopic signature indistinguishable from mid-ocean ridge basalt. This composition is unprecedented in the known volcanism from the Hawaiian hotspot, but is consistent with the interpretation from plate reconstructions[8] that the hotspot was located close to a mid-ocean ridge about 80 Myr ago. As the rising mantle plume encountered the hot, low-viscosity asthenosphere and hot, thin lithosphere near the spreading centre, it appears to have entrained enough of the isotopically depleted upper mantle to overwhelm the chemical characteristics of the plume itself. The Hawaiian hotspot thus joins the growing list of hotspots that have interacted with a rift early in their history.

For more than 81 Myr (ref. 9), the Hawaiian hotspot has been producing the age-progressive Hawaiian–Emperor chain of volcanic islands and seamounts (Fig. 1). This chain extends for 5,800 km from the present location of volcanic activity on the island of Hawaii and Loihi seamount, to the northernmost Emperor seamount (Meiji) at 53° N. There are over 100 volcanic edifices along the Hawaiian–Emperor chain, and more than 30 of these (in addition to the Hawaiian Islands) have been sampled by dredge and drill[9–11], making it the most intensively sampled and studied hotspot track on Earth.

Published Sr-isotope ratios of tholeiitic basalts from along the Hawaiian hotspot track show an interesting trend with age (Fig. 2). These ratios remain fairly constant along the Hawaiian Islands and the Hawaiian ridge between Kilauea volcano on Hawaii and Yuryaku seamount (Fig. 1); they then decrease steadily northwards along the Emperor seamounts to Suiko guyot, which was the oldest seamount previously analysed (64.7 Myr; ref. 12). This decrease in the $^{87}Sr/^{86}Sr$ ratio back in time was attributed to a decrease in distance between the hotspot and the nearest spreading centre[13]. Only the tholeiitic basalts (as opposed to the transitional and alkalic basalts) show this isotopic trend, perhaps because the tholeiites experienced little if any interaction with the lithosphere[14–16].

Because this trend in $^{87}Sr/^{86}Sr$ with time was all within the range for the Hawaiian Islands, it could be explained by a sampling bias in the older seamounts. We therefore decided to measure the isotopic ratios of basalts from the two oldest Emperor seamounts (Detroit and Meiji) to determine if the isotopic trend continued further back in time. We also analysed a single sample from Suiko to tie in with the published data. We chose to concentrate our analyses, and our discussion here, on the tholeiitic basalts because only they show the isotopic trend with time.

We measured the Sr, Nd and Pb isotope ratios of basalts from two locations (ODP Sites 883 and 884) on the Detroit seamount platform[9]. The Site 884 basalts have low concentrations of alkalis, TiO_2, and other incompatible elements at moderate MgO (4.6–8.8 wt%) and Ni (47–94 p.p.m.) contents, and are unambiguously tholeiitic[9]. Basalt recovered at the other drillsite on Detroit (Site 883) are too altered to determine unambiguously if they are tholeiitic (and we wish to limit our study to tholeiites); however, we include them here (Table 1) because they are isotopically similar to the Site 884 basalts (Fig. 3), which bolsters our argument that the Late Cretaceous volcanism was significantly different from the more recent volcanism. The Suiko sample from DSDP Site 433 and the Meiji sample from DSDP Site 192 are tholeiitic basalts[12,17].

Age-corrected (initial) $^{87}Sr/^{86}Sr$, $^{207}Pb/^{204}Pb$ and $^{208}Pb/^{204}Pb$ values (Table 1) in the Detroit tholeiites (Site 884) are lower than anything previously reported from the Hawaiian–Emperor chain (Fig. 3), while $^{143}Nd/^{144}Nd$ and $^{206}Pb/^{204}Pb$ values for these tholeiites overlap the Hawaiian field. Age corrections to these isotopic data are small (Table 1), and even the measured ratios are distinct from the Hawaiian data. The Sr and Pb isotope ratios of the Detroit tholeiites are within the range of Pacific mid-ocean-ridge basalt (MORB), while their $^{143}Nd/^{144}Nd$ values are lower than modern Pacific MORB, but within the range of Pacific MORB data adjusted to 80 Myr (Fig. 3b). Isotopic data for the Site 883 samples are similar to the Site 884 data, but are not quite as depleted.

The Suiko sample has the highest Sr and Pb isotope ratios measured in this study, and values of $^{143}Nd/^{144}Nd$ that are similar to those found at Meiji and Detroit (Table 1). Suiko isotopic ratios

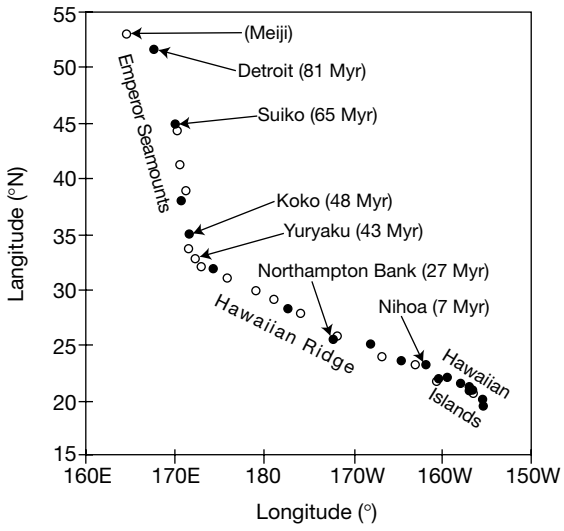

Figure 1 Location of volcanoes in the Hawaiian–Emperor island/seamount chain that have been dated (the age of Meiji is unknown). Additional locations have been sampled, but not dated. Locations from which tholeiites have been reported are shown by filled circles. Locations where no tholeiites were reported, or the identification of the tholeiites is in doubt, are shown by open circles. Seamounts mentioned in the text are labelled with names and ages. Age data are from a compilation[10], except for the Detroit seamount age[9]. New isotopic data presented in this study are from Suiko, Detroit and Meiji.